Evaluation of liquefaction/mudflow resistance of improved volcanic sandy ash soils focusing on dissipated energy

Y. KIYOHARA[(1)], M. KAZAMA[(2)]

[(1)] *Department of Civil Engineering and Architectural Design, National Institute of Technology, Hachinohe College, kiyohara-z@hachinohe-ct.ac.jp*
[(2)] *Department of Civil and Environmental Engineering, Graduate School of Engineering, Tohoku University, motoki.kazama.b2@tohoku.ac.jp*

Abstract

In the 2011 Tohoku earthquake, mudflow of residential land and failure of revetments and block retaining walls occurred off the Pacific Coast in the Aomori and Iwate prefectures. This study reports the investigation results of both damaged sites, and evaluates the liquefaction resistance of these soils by cyclic triaxial tests of saturated, undrained samples. Furthermore, the effectiveness of chemically grouted, cement-mixed, and well-compacted Shirasu soil specimens in terms of liquefaction resistance was validated by evaluating the dissipated energy. These improved Shirasu soils were tougher, and generated less excess pore water pressure owing to their positive dilatancy.

Keywords: liquefaction, cyclic triaxial test, dissipated energy, volcanic soil, chemical grouting

1. Introduction

In the 2011 Tohoku earthquake, mudflow of residential land and failure of revetments and block retaining walls occurred off the Pacific Coast, in the Aomori and Iwate prefectures [1, 2]. Both damage forms are thought to be similar to the liquefaction phenomena in volcanic sandy ash soils with high water contents. The grounds at both sites were constructed in the 1970s and 1980s by filling valleys with predominantly volcanic, porous, sandy soils containing pumice; these were transported from volcanos in the Quaternary Period; this soil is known as Shirasu in Japan. These soils have high water-retention capacities and crushable properties [3, 4]. A seismic intensity of 5 (Japanese Meteorological Agency) was observed around these areas during the earthquake. The acceleration records measured perpendicularly to the walls of each damaged site are shown in Figs. 1 and 2, respectively [5]. These maximum accelerations range from 80 to 130 gal. These values are not at a dangerous seismic level; however, these serious failures occurred. It is thought that the Shirasu's crushability and high-water retention property resulted in the serious failure.

Liquefaction strength curves obtained from cyclic triaxial tests are generally used to validate liquefaction-proof performance on ground. However, improved grounds like chemically grouted ones, which are tough and have not reached liquefaction, cannot be quantitatively evaluated in terms of proof performance by using the liquefaction curve. For this case, dissipated energy is thought to be an effective index with which to consider the proof performance of improved soil.

In this research, the triaxial cyclic behavior on soils from the damaged sites was investigated. Furthermore, the effectiveness of chemical grouting, cement mixing, and high compaction on liquefaction resistance was validated. By referencing the cyclic mobility, the accumulated dissipated energy was calculated and the results were compared with each other.

Photo 1 – Mudflow of residential land at Ninohe City

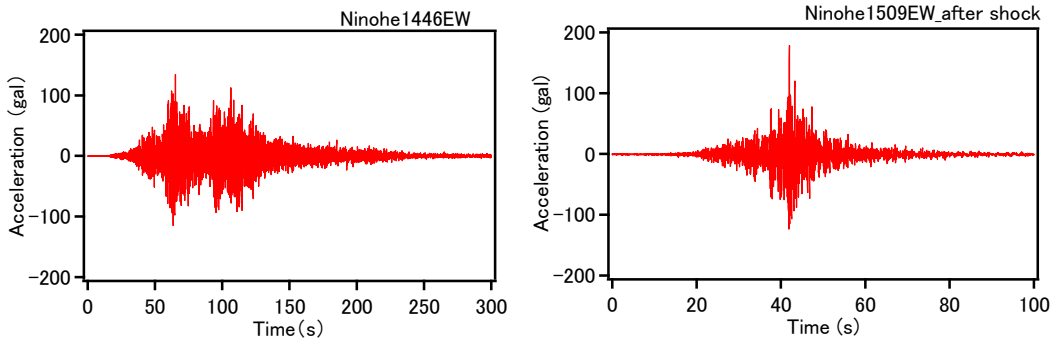

Fig. 1 – Ground acceleration record at Ninohe City (K-net Station Code IWT024)

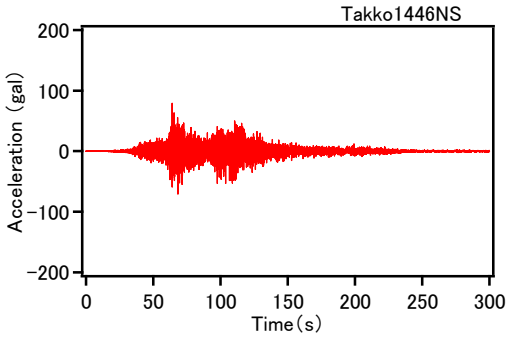

Fig. 2 – Ground acceleration record at Takko City (Kik-net Station Code AOMH18)

2. Experimental Method

2.1 Soil samples

The Ninohe Shirasu and Takko Shirasu soils sampled from each damaged site were sieved to less than 2 mm, and were respectively remolded using a 5-cm diameter and 10-cm height mold. The relative densities were adjusted to 60–65%. The soil physical properties are shown in Table 1. Photo 2 shows the Ninohe Shirasu sample surface imaged by SEM. The surface appears highly porous. The specific surface area measured by the BET method was approximately 12 m^2/g at Ninohe Shirasu, which is larger than that of silica sand No. 7 (0.5

m^2/g). Fig. 3 shows the particle size distribution. Each Shirasu sample contained approximately 35-38% fine particles. Compacted Shirasu tended to be refined by crushing and particle breakage.

Table 1 – Soil physical properties

	Silica sand No. 7	Ninohe Shirasu soil	Takko Shirasu soil
Soil density ρ_s (g/cm^3)	2.64	2.57-2.63	2.57
Maximum void ratio e_{max} [1)]	1.24	1.33	1.92
Minimum void ratio e_{min} [1)]	0.73	0.64	1.10
D_{50} (mm)	0.174	0.26	0.17
Fine content (%)	0	35	38.6
Surface area [2)] (m^2/g)	0.5	12.7	11.5

1) JIS A1224, 2) BET method.

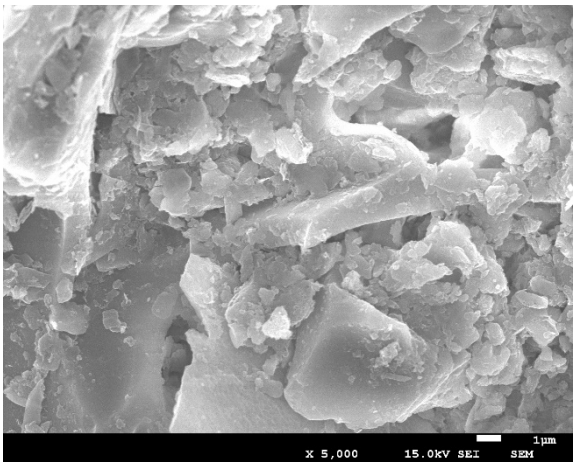

Photo 2 – Surface of Ninohe Shirasu particle (x5000)

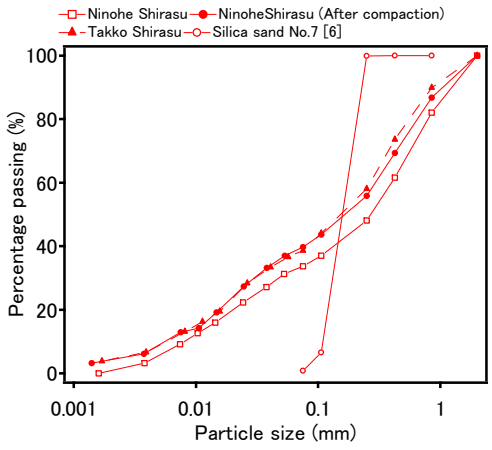

Fig. 3 – Particle size distribution curves

Furthermore, improved soils were prepared as follows: 5%-cement-mixed Ninohe Shirasu soil (CN), well-compacted Ninohe Shirasu soil with a relative density *D*r of 90% (DN), and chemically 7.2%-silica grouted Takko Shirasu soil (YT).

2.2 Cyclic Triaxial Test

Each specimen was set up on a stress-controlled cyclic triaxial test apparatus (Photo 3). After the saturation process of infiltrating de-aired water into the specimen, an isotropic consolidation pressure σ'_c of approximately 100 kPa was applied. Then, a cyclic deviator stress σ_d was applied under the saturated, undrained condition. The test conditions are shown in Table 2. This paper explains in detail the cyclic behavior of the following cases: σ_d = 29 kPa on Ninohe Shirasu (Nd29) [6]; σ_d = 39-77 kPa on cement-mixed Ninohe Shirasu (CNd39_77); σ_d = 75 kPa on well-compacted Ninohe Shirasu (DNd75); and σ_d = 44 kPa on Takko Shirasu (Td44), which liquefied after approximately 20 cycles. Moreover, the σ_d = 47-143 kPa of chemically grouted Takko Shirasu (YTd47_143) is also explained.

As shown in eq. (1), the normalized dissipated energy W was calculated for each experimental case by accumulating the multiplied deviator stress by axial deformation.

$$W = \Sigma \Delta W_i / \sigma'_0 = \Sigma q_i \Delta H_i \times 1000 / \sigma'_c \quad (1)$$

Therein, W is the normalized dissipated energy (J/m^2/kPa), σ'_0 the consolidation stress (kPa), q_i the deviator stress (kPa), ΔH_i the axial deformation (m), and i the partitioned number.

Photo 3 – Cyclic triaxial test apparatus

Table 2 – Cyclic triaxial test conditions

Soil name	Case name	Soil specimen		After consolidation			Cyclic triaxial test case		
		ρ_d (g/cm^3)	Void ratio	Void ratio	D_r (%)	B-value	Confining pressure σ_c' (kPa)	Deviator stress σ_d (kPa)	Frequency Hz
Ninohe Shirasu (N)	Nd19	1.35	0.90	0.85	68	0.92	97	19	0.5
	Nd26	1.39	0.84	0.79	77	0.94	96	26	0.5
	Nd29	1.40	0.84	0.77	79	0.98	100	29	0.5
	Nd33	1.38	0.87	0.81	74	0.95	100	33	0.5
	Nd38	1.38	0.86	0.81	74	0.94	100	38	0.5
Cement mixed Ninohe Shirasu (CN)	CNd39_77	1.37	0.92	0.90	66	1.00	100	39,58,77	0.1
	CNd59_70	1.38	0.91	0.89	68	1.02	100	59,70	0.1
	CNd75	1.38	0.91	0.89	67	1.00	100	75	0.1
	CNd77	1.37	0.91	0.91	65	—	100	77	0.1
	CNd89	1.37	0.93	0.91	64	0.96	100	89	0.1
Well-compacted Ninohe Shirasu (DN)	DNd75	1.50	0.71	0.66	97	0.74	87	75	0.5
	DNd86	1.50	0.71	0.66	98	0.72	88	86	0.5
	DNd93	1.48	0.74	0.68	95	0.67	88	93	0.5
	DNd103	1.51	0.70	0.65	98	0.79	88	103	0.5
	DNd115	1.52	0.69	0.64	100	0.70	88	115	0.5
Takko Shirasu (T)	Td36	0.96	1.67	1.47	55	0.97	100	36	0.5
	Td41	1.05	1.45	1.31	76	0.97	100	41	0.5
	Td44	1.05	1.46	1.33	75	0.98	100	44	0.5
	Td50	1.04	1.47	1.34	73	0.97	100	50	0.5
Chemically grouted Takko Shirasu (YT)	YTd47_143	1.17	1.19	1.17	91	0.97	100	47,97,143	0.5

□: Liquefied after approximately 20 cycles.

3. Experimental Results

Fig. 4 shows the conventional liquefaction strength curves obtained from the cyclic triaxial tests cases shown in Table 2. The liquefaction resistance of N-soil was smaller than that of silica sand No.7. The liquefaction strength rate to reach liquefaction after 20 cycles was approximately 0.15 on N-soil, 0.4 on CN-soil, 0.5 on DN-soil, and 0.22 on T-soil. The T-soil result was equal to that of standard sand [6]. YT-soil did not liquefy even at σ_d = 143 kPa. The liquefaction resistance of CN-soil was 2.7 times greater than that of N-soil.

Fig. 5 shows the stress-strain curves during cyclic loading in the σ_d case which liquefied after nearly 20 cycles, that is σ_d = 29 kPa on N-soil (Nd29), σ_d = 77 kPa on CN-soil (CNd39_77), σ_d = 75 kPa on DN-soil (DNd75), and σ_d = 44 kPa on T-soil (Td44). Furthermore, σ_d = 143 kPa on YT-soil (YTd47_143) is also shown in the figure. The axial strain ε_a of Nd29 and Td44 enlarged both the compression and extension sides, and the sample to liquefied after reaching a single-amplitude axial strain ε_a(SA) of approximately 2.5%. The maximum ε_a oscillated from -10% to 4% for Nd29, and from -6% to 10% for Td44.

To the contrary, in the CNd39_77 and DNd75 cases, compressive axial strain—which causes negative dilatancy and thus facilitates liquefaction—did not occur. And extensive axial strain proceeded, which caused positive dilatancy and reduced the generation of positive pore water pressure. For CNd39_77, ε_a ranged from -1% to 0% before liquefaction. YTd47_143 also remained within 1% during cyclic processing. It retained its elastic behavior for numerous cycles; then, extensive failure occurred without liquefaction. These specimens had improved deformation properties and toughness as a result of grouting or compaction.

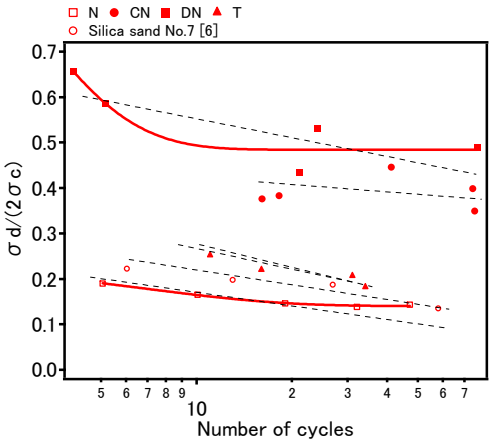

Fig. 4 – Liquefaction strength curve

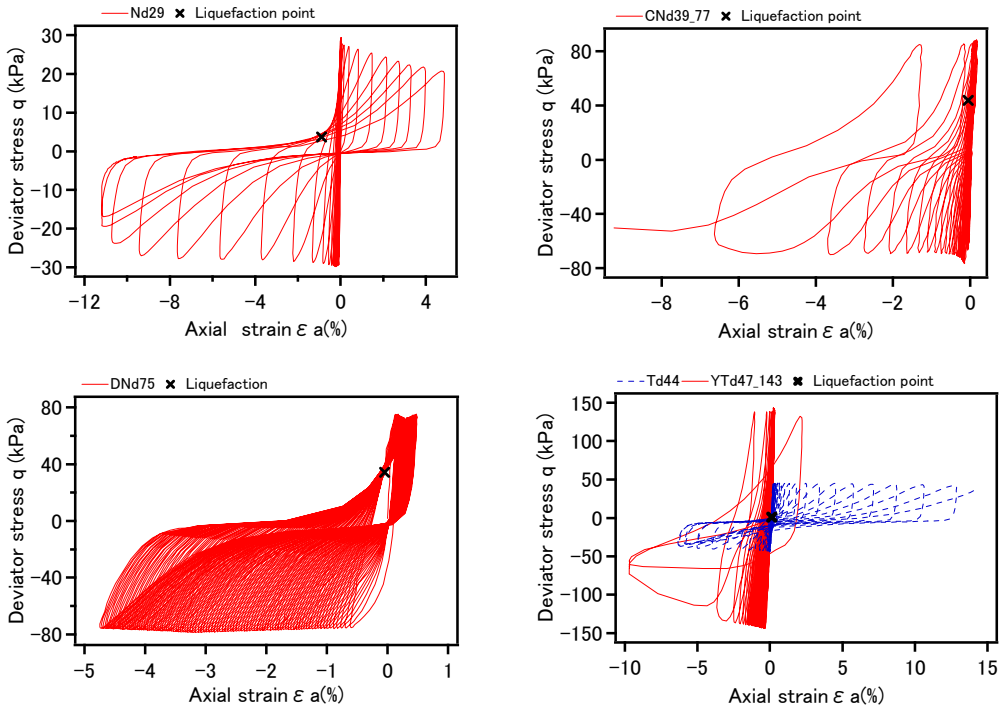

Fig. 5– Stress-strain curves of Nd29, CNd39_77, DNd75, Td44, and YTd47_143

Figs. 6 and 7 show the relation between ε_a(SA), excess pore water pressure, and dissipated energy for the case in which liquefaction occurred after nearly 20 cycles. During cyclic processing, the excess pore water pressures of CNd39_77 and DNd75 were reversed cyclically from positive values to nearly zero, which is attributable to the positive dilatancy effect. When the pore water pressure ratio R reached 0.95, W was calculated as approximately 1 J/m^2/kPa for Nd29, 3 J/m^2/kPa for CNd39_77, 11 J/m^2/kPa for DNd75, and 3 J/m^2/kPa for Td44. The required dissipated energy to reach ε_a(SA) = 2.5% was 1.8 J/m^2/kPa for Nd29, 80 J/m^2/kPa for DNd75 (after liquefaction), 3.7 J/m^2/kPa for Td44, and 27 J/m^2/kPa for YTd47_143. The

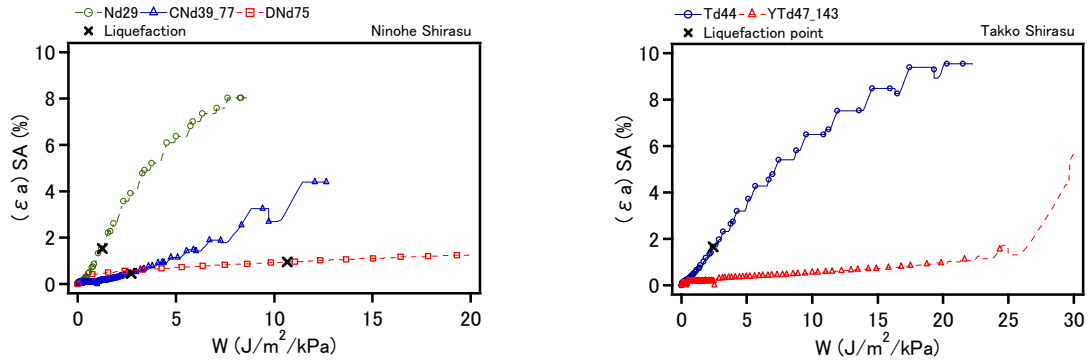

Fig. 6– Relation between single axial strain ε_a(SA) and dissipated energy for Nd29, CNd39_77, DNd93, Td44, and YTd47_143

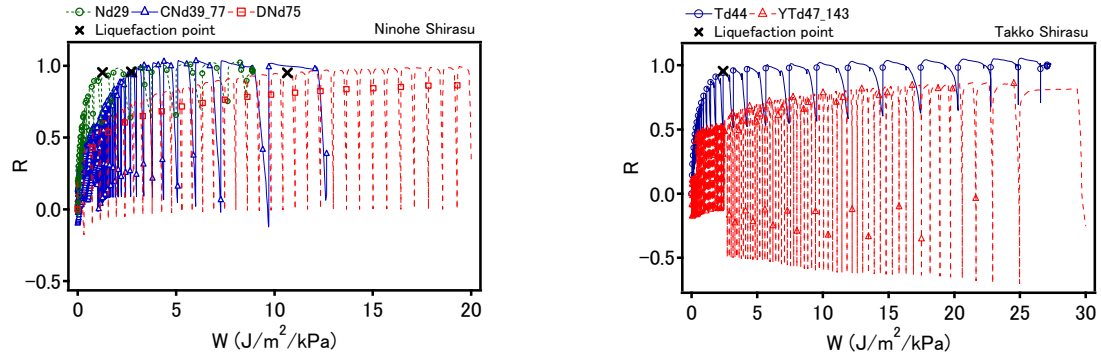

Fig. 7– Relation between excess pore water pressure and dissipated energy for Nd29, CNd39_77, DNd75, Td44, and YTd47_143

dissipated energy of improved soils (DNd75, YTd47_143) was 8-44 times greater than that of unimproved soils. In this study, compaction (DNd75) was the most effective way to prevent liquefaction.

Fig. 8 shows the relation between liquefaction strength rate ($\sigma_d/2\sigma'_0$) and dissipated energy. When liquefaction occurred in the improved soils, more than 2.5 J/m^2/kPa of dissipated energy was required. This value corresponds to a $\sigma_d/2\sigma'_0$ of 0.35, which was calculated from the earthquake acceleration and overburden pressure using eq. (2).

$$FL=(\sigma_d/2\sigma'_0)_{N=20}/(r_d\, A_{max}/g\cdot\sigma_v/\sigma'_v) \qquad (2)$$

where FL is the safety factor, $(\sigma_d/2\sigma'_0)_{N=20}$ the liquefaction strength rate liquefied after 20 cycles, N the cyclic time, r_d the correction factor (0.85), A_{max} the maximum acceleration (200 gal), g the gravitational acceleration (981 gal), σ_v the overburden pressure (96 kPa), and σ'_v the effective overburden pressure (48 kPa).

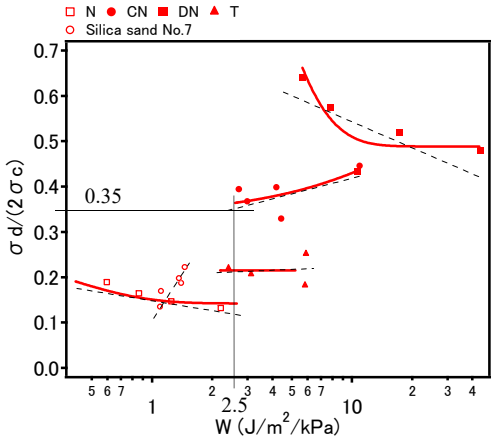

Fig. 8– Relation between deviator stress ratio and dissipated energy

4. Conclusion

Stress-controlled triaxial cyclic tests were performed on crushable Shirasu soil. Although Shirasu soil contains approximately 35% fine particles, the liquefaction strength was equal or smaller than that of standard silica sand. Moreover, these specimens had increased axial strain and a negative dilatancy. In contrast, the grouted and compacted Shirasu soils did not generate compressive strain and negative dilatancy. The excess pore water pressure oscillated from positive to negative, and the ground improvement contributed to the soil toughness. The dissipated energy required to reach liquefaction of the well-compacted and chemically grouted Shirasu soil was 8-44 times greater than that of the unimproved soil. In terms of dissipated energy, compaction was the most effective way to improve the earthquake-proof performance on Shirasu ground. The relation between the dissipated energy and the liquefaction strength rate $\sigma'_d/2\sigma'_0$ was clarified for a given acceleration and overburden pressure.

Acknowledgements

This work was supported by JSPS KAKENHI Grant Number Jp18K04356, 18H0152901, 16K0649501.

References

[1] Joint editorial committee for the report on the great east Japan earthquake disaster (2014): *Report on the Great East Japan Earthquake Disaster-Fudamental Aspects3 Geohazards*. Maruzen.

[2] Kazama M., Kawai T., Kim J., and Tomita M. (2015): Subjects of the liquefaction research seen to the liquefaction damage of the Great East Japan Earthquake Disaster, *J. Japan Association for Earthquake Engineering*, 15-7, pp.49-59.

[3] Kazama M., Takamura H., Unno T., Sento N., and Uzuoka R. (2006): Liquefaction Mechanism of Unsaturated Volcanic Sandy Soils, *Journal of JSCE* C, vol.62, no.2, pp.546-561.

[4] Kiyohara Y. and Kazama M. (2016): Liquefaction strength of volcanic sandy soil (SHIRASU) – Mudflow-type slope failure on the 2011 off the Pacific Coast of Tohoku Earthquake –, 7th *Taiwan-Japan Workshop on Geotechnical Hazards from Large Earthquakes and Heavy Rainfall*, pp.89-90, PingTung, Taiwan.

[5] National Research Institute for Earth Science and Disaster Resilience (2019): NIED K-NET, KiK-net,National Research Institute for Earth Science and Disaster Resilience, doi:10.17598/NIED.0004.

[6] Kiyohara Y. (2016): Cyclic undrained triaxial tests for liquefaction strength and deformation properties of saturated and unsaturated Ninohe Shirasu, *Journal of JSCE* C, Vol.72, No.3, pp.196-203.

